Clim. Past Discuss., 11, 1551–1578, 2015
www.clim-past-discuss.net/11/1551/2015/
doi:10.5194/cpd-11-1551-2015

Climate of the Past Discussions
Open Access

Stability of the vegetation–atmosphere system in the early Eocene climate

U. Port[1] **and M. Claussen**[1,2]

[1]Max Planck Institute for Meteorology, Hamburg 20146, Germany
[2]Meteorological Institute, University of Hamburg, Hamburg 20146, Germany

Received: 26 March 2015 – Accepted: 21 April 2015 – Published: 5 May 2015

Correspondence to: U. Port (ulrike.port@mpimet.mpg.de)

Published by Copernicus Publications on behalf of the European Geosciences Union.

Abstract

We explore the stability of the atmosphere–vegetation system in the warm, almost ice-free early Eocene climate and in the interglacial, pre-industrial climate by analysing the dependence of the system on the initial vegetation cover. The Earth system model of the Max Planck Institute for Meteorology is initialised with either dense forests or bare deserts on all continents. Starting with desert continents, an extended desert remains in Central Asia in early Eocene climate. Starting with dense forest coverage, this desert is much smaller because the initially dense vegetation cover enhances water recycling in Central Asia relative to the simulation with initial deserts. With a smaller Asian desert, the Asian monsoon is stronger than in the case with a larger desert. The stronger Asian monsoon shifts the global tropical circulation leading to coastal subtropical deserts in North and South America which are significantly larger than with a large Asian desert. This result indicates a global teleconnection of the vegetation cover in several regions. In present-day climate, a bi-stability of the atmosphere–vegetation system is found for Northern Africa only. A global teleconnection of bi-stabilities in several regions is absent highlighting that the stability of the vegetation–atmosphere system depends on climatic and tectonic boundary conditions.

1 Introduction

The interaction between atmosphere and vegetation may allow for multiple equilibria of the vegetation–atmosphere system pointing to intransitive dynamics in the climate system is as suggested by Lorenz (1968). Multiple equilibrium states have been detected in various model simulations when initialised with different vegetation covers. Claussen (1994, 1998), Claussen and Gayler (1997), Kubatzki and Claussen (1998), Wang and Eltahir (2000), Zeng and Neelin (2000), and Rachmayani et al. (2015) find multiple state in Northern Africa, Oyama and Nobre (2003) in the Amazon region, Claussen (1998) in Central Asia, and Dekker et al. (2010) in the northern high latitudes. In all cases,

CPD
11, 1551–1578, 2015

simulations with initially more extended vegetation cover lead to a moister climate and smaller deserts than simulations initialised with sparse vegetation coverage.

The stability of the atmosphere–vegetation system depends on the climate state. For example, the intransitivity of the atmosphere–vegetation system over Northern Africa vanishes, or becomes much less pronounced, for the mid-Holocene climate in the simulations by Claussen and Gayler (1997) and Rachmayani et al. (2015), respectively. Likewise, Bathiany et al. (2012) show that the pattern of bi-stability over Northern Africa changes at different times in different location during the transition from mid to late Holocene. Such changes in the stability of the atmosphere–vegetation system may lead to abrupt changes in vegetation and climate due to a loss of stability in the regions which exhibit multiple states (Brovkin et al., 1998; Claussen et al., 1999; Renssen et al., 2003). Further, changes in the stability of the atmosphere–vegetation system may even induce abrupt changes in locations which seem to be more stable, but which are interlinked with the unstable locations (Bathiany et al., 2013a, b).

So far, most studies have assessed the stability of the atmosphere–vegetation system for interglacial or glacial climate, i.e. a climate states with permanent ice sheets. Little is known about the transitivity of the atmosphere–vegetation system in climates that strongly differ from the current late Quaternary climate. Therefore, we explore the stability of the atmosphere–vegetation system in climate of the early Eocene. The early Eocene (about 54 to 52 Ma ago) belongs to the warmest periods in the last 65 million years. An atmospheric CO_2 concentration between 300 and 2000 ppm (Beerling and Royer, 2011) as well as a different orography and bathymetry than today led to 5 °C to 6 °C warmer tropics (Pearson et al., 2007) and to mostly ice-free poles (Zachos et al., 1992). The warm climate allowed a dense vegetation cover in almost all regions (Willis and McElwain, 2002). Even on Antarctica and in the high North, flora fossils indicate a dense tree cover (Wolfe, 1985; Eberle and Greenwood, 2012; Harrington et al., 2012; Pross et al., 2012).

Using the Earth system model of the Max Planck Institute for Meteoroloy (MPI-ESM), we simulate the early Eocene climate and the pre-industrial climate. We start simula-

CPD
11, 1551–1578, 2015

tions from two different vegetation states, all ice-free continents are either completely covered with dense forests or with bare-soil deserts, respectively (Port et al., 2015). From these initial states, the model system is allowed to freely evolve, with dynamically interacting atmosphere, ocean, and vegetation. Depending on the initial conditions, new equilibria in the vegetation–atmosphere system are reached after some 1000 years of simulation.

2 Experiment

2.1 Model

The Earth system model of the Max Planck Institute for Meteorology (MPI-ESM) consists of the atmospheric general circulation model ECHAM6 (Stevens et al., 2013), the Max Planck Institute Ocean Model MPIOM (Jungclaus et al., 2013), the land surface scheme JSBACH (Reick et al., 2013), and the ocean biogeochemistry model HAMOCC (Ilyina et al., 2013). We use ECHAM6 in a horizontal resolution is T31 (approximately 3.75°) and with 31 levels in the vertical. The ocean grid has a horizontal resolution of about 3° and 40 levels in depth.

JSBACH includes a dynamic vegetation module based on a tiling approach (Brovkin et al., 2009). Vegetation is represented by eight Plant Functional Types (PFTs) which reflect present-day plant taxa (Table 1). During the early Eocene, however, plant types have been differed from today. Grass land is common today, but it did not exist during the early Eocene (Willis and McElwain, 2002). C_3 spreaded in the early to mid Miocene (20–10 Ma) (Janis, 1993), while C_4 expanded during the mid to late Miocene (Cerling et al., 1993). Instead, other plant species dominated the vegetation cover during the early Eocene which are extinct, or almost extinct, today such as paratropical rainforest or polar forest (Wolfe, 1985). In our study, we neglect any differences in plant taxa. Thus, we focus on the biogeophysical processes and their differences between early

CPD
11, 1551–1578, 2015

Eocene and pre-industrial climate. The effect of difference between early Eocene and current plant taxa will be the focus of subsequent studies.

2.2 Early Eocene setting

For our early Eocene simulations, we use the same boundary conditions as Port et al. (2015). Orography and bathymetry are based on the maps by Bice and Marotzke (2001) which Heinemann et al. (2009) interpolated from the original resolution of 2° times 2° to the model resolution of T31. The orography map lacks information on sub-grid orography such as slope, anisotropy, orientation, SD, maxiumum, minimum, mean elevation. Without these informations, sub-grid interactions of atmospheric flow with orography can not be parameterised in ECHAM6 (Stevens et al., 2013). Hence, we turn off the module for sub-grid orographic drag and wave generation.

In the standard version of MPIOM, the grid poles are over Greenland and Antarctica. With Eocene continents, the pole over present-day Greenland coincide with the Palaeo-Atlanic Ocean, i.e. meridians converge at this pole leading to numerical singularies. To avoid singularies, we use the setting by Heinemann et al. (2009) who placed the MPIOM north pole and south pole to the large continents of Palaeo-Asia and to Palaeo-South America, respectively.

The atmospheric CO_2 concentration is fixed to 560 ppm (Table 2), which is the lower limit of reconstructions (Zachos et al., 2001; Beerling and Royer, 2011). Methane and nitrous oxide are set to pre-industrial values in the early Eocene atmosphere and also the orbit corresponds to the pre-industrial orbit (Table 2). This approach limits the differences between the early Eocene and the pre-industrial boundary conditions to the distribution of continents, the bathymetry, the presence of ice sheets, and the atmospheric CO_2 concentration.

CPD
11, 1551–1578, 2015

2.3 Simulations

Our simulations start from the simulations by Port et al. (2015). They explore the impact of extreme land cover on the early Eocene climate and the pre-industrial climate by simulating and a "desert world" and a "forest world" for both climates, respectively. In the "desert world", no vegetation occurs on all continents during the simulated 400 years. In the "forest world", trees cover all ice-free continents completely.

In order to separate the albedo effect of vegetation from the hydrological effect, Port et al. (2015) simulate the forest world and the desert world two times, respectively. All soils either have a homogeneous albedo of 0.1 (dark soil) or 0.4 (bright soil). In the dark soil case, soil and vegetation have about the same albedo leading to weak albedo changes by vegetation relative to bare soil. In other words, vegetation affects climate mainly through the hydrological cycle. In the bright soil case, vegetation has a much lower albedo than soil. Hence, both, the albedo effect and the hydrological effect of vegetation are pronounced.

At the end of the simulations by Port et al. (2015), climate differs significantly between the forest worlds and the desert worlds. We extend those simulations by further 1000 years. During the extended simulations, atmosphere, ocean, and vegetation interact and thus, vegetation establishes, migrates, and retreats dynamically. In the bright-soil simulations, the vegetation–atmosphere system reaches the same state when initialised with dense forest as when initialised with bare soil. As we focus on intransitive dynamics in the vegetation–atmosphere system, we exclude a detailed discussion of the bright-soil simulations in this study. Instead, we present the results for the dark-soil simulations where multiple equilibria establish depending on the initial vegetation cover in both, the early Eocene and the pre-industrial climate. Table 3 gives an overview of the considered four simulations where all soils have a low soil albedo.

CPD
11, 1551–1578, 2015

3 Results and discussion

3.1 Early Eocene climate

The warm and humid early Eocene climate favours dense vegetation cover in almost all regions. Only in Central Asia and in southern Africa, deserts remain in the DE simulation (Fig. 1). Subtropical semi-deserts establish in South America, North America, and Australia. In these arid and semi-arid regions, pronounced differences in vegetation cover emerges between the DE simulation and the FE simulation (Fig. 2).

In the semi-desert in western North America (marked in Fig. 2), the desert cover is larger by 0.43 in the FE simulation than in the DE simulation and precipitation is smaller by 0.52 mm day^{-1} (70 %) (Fig. 3c). In the semi-desert in southern South America, desert cover is larger by 0.19 and precipitation is smaller by 0.5 mm day^{-1} (43 %) in the FE simulation (Fig. 3b). The differences on the American continents are counterintuitive because starting from dense forest leads to a larger desert in these regions than starting from bare soil. This result disagrees with all simulations previously mentioned in the introduction. Later, we will discuss the mechanism causing these bi-stabilities.

In the semi-desert in southern Africa (marked in Fig. 2), desert cover is smaller by 0.12 at the end of the FE simulation than at the end of the DE simulation (Fig. 3d). However, considering the trend of −0.04 and 0.07 per 100 years at the end of the FE and DE simulation, the difference in vegetation cover may not be significant.

In the Asian desert, the differences in the vegetation cover are most pronounced. At the southern edge of the desert, more grass and trees remain in the FE simulation than in the DE simulation (Fig. 2). At the beginning of the FE simulation, the dense forest transpires 1.35 mm day^{-1} leading to an evapotranspiration of 1.7 mm day^{-1} and a precipitation of 1.8 mm day^{-1} in Central Asia (Fig. 3a). During the FE simulation, precipitation is sufficient to maintain a large part of the vegetation cover which preserves high transpiration rates and strong precipitation. By the end of the FE simulation, desert cover amounts to 0.43 and precipitation to 0.82 mm day^{-1} in Central Asia.

CPD
11, 1551–1578, 2015

At the beginning of the DE simulation, evapotranspiration in Central Asia is ten times weaker than at the beginning of the FE simulation and precipitation is six times smaller (Fig. 3a). Starting from this dry climate, only little vegetation establishes preserving a dry climate in Central Asia. At the end of the DE simulation, desert cover in Central Asia is larger by 0.36 than in the FE simulation and precipitation weaker by $0.6\,\mathrm{mm\,day^{-1}}$.

In both, the FE and the DE simulation, soil have an albedo of 0.1 which is similar to the albedo of vegetation. Hence, the albedo effect of vegetation is weak and the multiple stable vegetation–atmosphere states in Central Asia result from a hydrological feedback. As vegetation increases precipitation in Central Asia mostly during the Asian monsoon (Fig. 4), we suggest that vegetation enhances water recycling leading a stronger Asian monsoon and to more precipitation relative to bare soil and feeding back to vegetation growth.

Above, we show that the semi-deserts on the American continents are larger in the simulation with initial forest cover than in the simulation with initial desert. To identify the driving mechanism for this bi-stability, we analyse the impact of vegetation on the large scale atmospheric circulation in further detail. Following Claussen (1997), we compute the velocity potential at 200 hPa which is an indicator of large scale, upper-air divergence and convergence, and hence, convection and subsidence in the tropics. The separation of the horizontal wind, V, in the rotational component, V_Ψ, and in the divergent component, V_χ, yields

$$V = V_\Psi + V_\chi. \tag{1}$$

The divergent part of the wind is the gradient of the velocity potential, χ,

$$\nabla\chi = V_\chi. \tag{2}$$

Hence, the divergent part of the large scale wind is directed towards the strongest increase in the velocity potential. This relation implies that air flows from the centre of negative velocity potential to the centre of positive velocity potential. Therefore, upper

CPD
11, 1551–1578, 2015

air diverges in the centre of negative velocity potential and converges in the centre of positive velocity potential. Below the divergence, air rises and below the convergence, air subsides.

Figure 5a shows a bipolar pattern in the velocity potential at 200 hPa at the end of the DE simulation. The centre of positive velocity potential indicates subsidence over the tropical Atlantic Ocean, while the centre of negative velocity potential implies convection over the western Pacific Ocean. Over Central Asia, positive velocity potential prevails indicating subsidence over this region.

In the FE simulation, velocity potential pattern differs from the DE simulation (Fig. 5b). In Central Asia more vegetation remains in the FE simulation than in the DE simulation. The additional vegetation enhances convection over this region as indicated by the negative velocity potential. With a stronger convection over Asia, the amplitude of the velocity potential pattern increases and the pattern shifts westwards relative to the DE simulation indicating different large scale atmospheric circulations in both simulations.

With a different global atmospheric circulation, precipitation differs significantly between the FE and the DE simulation (Fig. 6). At the west coast of the American continents, precipitation is weaker in the FE simulation leading to less vegetation in the semi-arid regions in western North America and southern South America. In other words, the multiple vegetation–atmosphere states in these semi-arid regions seem to be connected to the multiple vegetation–atmosphere states in Central Asia.

Such a connection of multiple vegetation states in several regions, so far, has not been found for the present-day climate. Claussen (1997) simulates a shift in the atmospheric circulation with different vegetation states in the Sahara. However, the shifted atmospheric circulation affects the vegetation in the Sahara only.

The question remains which mechanism links the multiple stable vegetation states in Central Asia and on the American continents. Both regions are connected through the Walker circulation. In the present-day climate, the Walker circulation describes the zonal atmospheric circulation over the subtropical Pacific Ocean. In combination

CPD
11, 1551–1578, 2015

with the zonal ocean circulation in the Pacific Ocean, the Walker circulation forms the El Niño–Southern Oscillation.

In the early Eocene simulations, the strong bipolar pattern in the velocity potential is associated with a zonal circulation similar to the tropical Walker circulation today: air rises over the western Pacific Ocean and subsides over the eastern Pacific Ocean (Fig. 5). In the FE simulation, this bipolar pattern is more pronounced indicating that vegetation in central Asia enhances the convection branch of the Walker circulation relative to the DE simulation. Due to continuity reasons, stronger convection in Asia causes stronger subsidence over the American continents and, therefore, less vegetation in the American subtropics.

3.2 Pre-industrial climate

In the pre-industrial Sahel, more vegetation remains in the FP simulation than establishes in the DP simulation (marked region in Fig. 2). Time series of desert cover and precipitation in the Sahel illustrate that desert cover is smaller by 0.21 at the end of the FP simulation than at the end of the DP simulation and precipitation is about two times stronger (Fig. 7).

In comparison to the stability of the vegetation–atmosphere system in the early Eocene climate, only the vegetation in the Sahel is bistable indicating that globally connected bi-stabilties in several regions are absent in the pre-industrial climate. To identify the reason for the different stability of the vegetation–atmosphere system in the early Eocene and in the pre-industrial climate, we analyse the velocity potential at 200 hPa in Fig. 8. The positive velocity potential over the Sahel implies that subsidence prevails over this region. Even the additional vegetation in the FP simulation does not enhance convection. Presumably, the subsidence over the Sahel prevents vegetation from inducing strong convection.

As vegetation fails to enhance convection over the Sahel, the global atmospheric circulation is almost the same in the FP simulation and the DP simulation leading to only weak differences in precipitation between both simulations (Fig. 9). Especially outside

CPD
11, 1551–1578, 2015

Northern Africa and over continents, precipitation differences are small. Hence, further multiple stable vegetation states in other regions than Northern Africa are absent.

In short, the large scale atmospheric circulation limits the multiple stable vegetation–atmosphere states to North Africa. In the early Eocene climate, the bi-stability in central Asia affects subtropical deserts on the American continents because the atmospheric circulation allows vegetation in Central Asia to enhance the Asian monsoon and to shift global atmospheric circulation. The different stability of the vegetation–atmosphere system in the early Eocene and in the pre-industrial climate indicates that the location of the bi-stability relative to the atmospheric circulation determines the large scale extent of the bi-stability.

As a final note, we point to the sensitivity of our results to the soil albedo. We here assume a soil albedo of 0.1 which is almost the same as the albedo of vegetation. Due to the low soil albedo, we exclude the albedo effect of vegetation and isolate the hydrological effect. Previous studies identified the albedo effect as the major driver for multiple stable vegetation–atmosphere states in the Sahel (Charney, 1975; Charney et al., 1977; Claussen and Gayler, 1997). Other than in those studies, the bi-stabilities in our study are driven by the hydrological effect of vegetation highlighting the importance of the hydrological effect.

4 Conclusions

In our early Eocene simulation, we have found multiple climate states that emerge from the intransitivity of the global climate system which are triggered by different initial conditions. These multiple states differ from those detected in similar simulations of the pre-industrial climate. In the simulations of the early Eocene climate, a desert in Central Asia is much larger in simulations initialised with bare continents than in simulations initialised with densely forested continents. This difference results from the interdepence of vegetation and precipitation leading to a positive hydrological feedback. Most notably, the large-scale atmospheric circulation differs for the different initial

CPD
11, 1551–1578, 2015

vegetation covers which leads to larger coastal deserts in North and South America in the simulation with initially forested continents.

In our simulations, we focused on the biogeophysical processes and associated intransitivity of the atmosphere–vegetation system. We neglected any differences between plant taxa and used pre-industrial plant functional types (PFTs) for the early Eocene climate simulation. We assume that adjusting PFTs to early Eocene taxa will not change our results drastically even though the bi-stability in the Asian vegetation cover is associated with grasses. Grasses ocurred rarely during the early Eocene but, from the modelling point of view, grass behaves similar to herbs and fern which grew plentifully during that time (Utescher and Mosbrugger, 2007). Testing the sensitivity of our results to the used PFTs is subject to future studies.

In our pre-industrial simulations, the multiple stable vegetation–atmosphere states are predominately limited to Northern Africa. With the present-day distribution of continents, subsidence prevails over Northern Africa, and vegetation induces only weak convection thereby affects the large-scale atmospheric circulation only marginally. During the early Eocene, however, an Asian desert forms which is located in a region with large-scale upper-air divergence. In this region, vegetation induces convection and shifts large scale atmospheric circulation leading to further multiple stable vegetation states on the American continents.

The different regional extent of multiple vegetation–atmosphere states in the early Eocene climate and in the pre-industrial climate suggest that climate and distribution of continents determines the stability of the vegetation–atmosphere system as well as the mechanisms causing multiple stable vegetation–atmosphere states. Understanding the sensitivity of multi-stabilities to constantly changing boundary contitions, such as climate and continents, deepens our knowledge about intransitive dynamcis in the climate system.

Acknowledgements. We thank Veronika Gayler and Helmuth Haak for technical support and the anonymous reviewer their heplful comments on this paper. This work used computational recources by Deutsches Klima Rechenzentrum (DKRZ) and was supported by the Max Planck

CPD
11, 1551–1578, 2015

Gesellschaft (MPG).

The article processing charges for this open-access publication were covered by the Max Planck Society.

References

Bathiany, S., Claussen, M., and Fraedrich, K.: Implications of climate variability for the detection of multiple equilibria and for rapid transitions in the atmosphere–vegetation system, Clim. Dynam., 38, 1775–1790, 2012. 1553

Bathiany, S., Claussen, M., and Fraedrich, K. F.: Detecting hotspots of atmosphere–vegetation interaction via slowing down. part 1: A stochastic approach, Earth System Dynamics, 4, 63–78, 2013a. 1553

Bathiany, S., Claussen, M., and Fraedrich, K.: Detecting hotspots of atmosphere–vegetation interaction via slowing down – part 2: Application to a global climate model, Earth System Dynamics, 4, 79–93, 2013b. 1553

Beerling, D. and Royer, D.: Convergent Cenozoic CO_2 history, Nat. Geosci., 4, 418–420, 2011. 1553, 1555

Bice, K. L. and Marotzke, J.: Numerical evidence against reversed thermohaline circulation in the warm Paleocene/Eocene ocean, J. Geophys. Res., 106, 11529–11542, 2001. 1555, 1568

Brovkin, V., Claussen, M., Petoukhov, V., and Ganopolski, A.: On the stability of the atmosphere–vegetation system in the Sahara/Sahel region, J. Geophys. Res.-Atmos., 103, 31613–31624, 1998. 1553

Brovkin, V., Raddatz, T., and Reick, C. H.: Global biogeophysical interactions between forest and climate, Geophys. Res. Lett., 36, L07405, doi:10.1029/2009GL037543, 2009. 1554

Cerling, T., Wang, Y., and Quade, J.: Expansion of C_4 ecosystems as an indicator of global ecological change in the late Miocene, Nature, 361, 344–345, 1993. 1554

Charney, J., Quirk, W., Chow, S., and Kornfield, J.: Comparative-study of effects of albedo change on drought in semi-arid regions, J. Atmos. Sci., 34, 1366–1385, 1977. 1561

Charney, J. G.: Dynamics of deserts and drought in Sahel, Q. J. Roy. Meteorol. Soc., 101, 193–202, 1975. 1561

CPD
11, 1551–1578, 2015

Claussen, M.: On coupling global biome models with climate models, Clim. Res., 4, 203–221, 1994. 1552
Claussen, M.: Modeling bio-geophysical feedback in the African and Indian monsoon region, Clim. Dynam., 13, 247–257, 1997. 1558, 1559
Claussen, M.: On multiple solutions of the atmosphere–vegetation system in present-day climate, Glob. Change Biol., 4, 549–559, 1998. 1552
Claussen, M. and Gayler, V.: The greening of the Sahara during the mid-Holocene: results of an interactive atmosphere–biome model, Global Ecol. Biogeogr., 6, 369–377, 1997. 1552, 1553, 1561
Claussen, M., Kubatzki, C., Brovkin, V., Ganopolski, A., Hoelzmann, P., and Pachur, H.-J.: Simulation of an abrupt change in Saharan vegetation in the mid-Holocene, Geophys. Res. Lett., 26, 2037–2040, 1999. 1553
Dekker, S. C., de Boer, H. J., Brovkin, V., Fraedrich, K., Wassen, M. J., and Rietkerk, M.: Biogeophysical feedbacks trigger shifts in the modelled vegetation–atmosphere system at multiple scales, Biogeosciences, 7, 1237–1245, doi:10.5194/bg-7-1237-2010, 2010. 1552
Eberle, J. J. and Greenwood, D. R.: Life at the top of the greenhouse Eocene world – a review of the Eocene flora and vertebrate fauna from Canada's high Arctic, Geol. Soc. Am. Bull., 124, 3–23, 2012. 1553
Harrington, G. J., Eberle, J., Le-Page, B. A., Dawson, M., and Hutchison, J. H.: Arctic plant diversity in the early Eocene greenhouse, P. Roy. Soc. B-Biol. Sci., 279, 1515–1521, 2012. 1553
Heinemann, M., Jungclaus, J. H., and Marotzke, J.: Warm Paleocene/Eocene climate as simulated in ECHAM5/MPI-OM, Clim. Past, 5, 785–802, doi:10.5194/cp-5-785-2009, 2009. 1555
Ilyina, T., Six, K. D., Segschneider, J., Maier-Reimer, E., Li, H., and Nunez-Riboni, I.: Global ocean biogeochemistry model HAMOCC: model architecture and performance as component of the MPI-Earth System Model in different CMIP5 experimental realizations, J. Adv. Model. Earth Syst., 5, 287–315, 2013. 1554
Janis, C. M.: Tertiary mammal evolution in the context of changing climates, vegetation, and tectonic events, Annu. Rev. Ecol. Syst., 24, 467–500, 1993. 1554
Jungclaus, J. H., Fischer, N., Haak, H., Lohmann, K., Marotzke, J., Matei, D., Mikolajewicz, U., Notz, D., and von Storch, J. S.: Characteristics of the ocean simulations in the Max Planck Institute Ocean Model (MPIOM) the ocean component of the MPI-Earth system model, J. Adv. Model. Earth Syst., 5, 422–446, 2013. 1554

CPD
11, 1551–1578, 2015

Kubatzki, C. and Claussen, M.: Simulation of the global bio-geophysical interactions during the last glacial maximum, Clim. Dynam., 14, 461–471, 1998. 1552
Lorenz, E.: Climatic determinism, Meteor. Mon., 8, 1–3, 1968. 1552
Oyama, M. and Nobre, C.: A new climate–vegetation equilibrium state for tropical South America, Geophys. Res. Lett., 30, 23, doi:10.1029/2003GL018600, 2003. 1552
Pearson, P., van Dongen, B., Nicholas, C., Pancost, R., and Schouten, S.: Stable warm tropical climate through the Eocene epoch, Geology, 35, 211–214, 2007. 1553
Port, U., Claussen, M., and Brovkin, V.: Radiative forcing by forest and subsequent feedbacks in the early Eocene climate, Clim. Past Discuss., 11, 997–1029, doi:10.5194/cpd-11-997-2015, 2015. 1554, 1555, 1556, 1569
Pross, J., Contreras, L., Bijl, P. K., Greenwood, D. R., Bohaty, S. M., Schouten, S., Bendle, J. A., Röhl, U., Tauxe, L., Ian Raine, J., Huck, C. E., van de Flierdt, T., Jamieson, S. S. R., Stickley, C. E., van de Schootbrugge, B., Escutia, C., Brinkhuis, H., and Program, I. O. D.: Persistent near-tropical warmth on the antarctic continent during the early Eocene epoch, Nature, 488, 73–77, 2012. 1553
Rachmayani, R., Prange, M., and Schulz, M.: North African vegetation–precipitation feedback in early and mid-Holocene climate simulations with CCSM3-DGVM, Clim. Past, 11, 175–185, doi:10.5194/cp-11-175-2015, 2015. 1552, 1553
Reick, C. H., Raddatz, T., Brovkin, V., and Gayler, V.: Representation of natural and anthropogenic land cover change in MPI-ESM, J. Adv. Model. Earth Syst., 5, 459–482, 2013. 1554
Renssen, H., Goosse, H., and Fichefet, T.: On the non-linear response of the ocean thermohaline circulation to global deforestation, Geophys. Res. Lett., 30, 1061, doi:10.1029/2002GL016155, 2003. 1553
Stevens, B., Giorgetta, M., Esch, M., Mauritsen, T., Crueger, T., Rast, S., Salzmann, M., Schmidt, H., Bader, J., Block, K., Brokopf, R., Fast, I., Kinne, S., Kornblueh, L., Lohmann, U., Pincus, R., Reichler, T., and Roeckner, E.: Atmospheric component of the MPI-M Earth System Model: ECHAM6, J. Adv. Model. Earth Syst., 5, 146–172, 2013. 1554, 1555
Utescher, T. and Mosbrugger, V.: Eocene vegetation patterns reconstructed from plant diversity – a global perspective, Palaeogeogr. Palaeocl., 247, 243–271, 2007. 1562
Wang, G. and Eltahir, E.: Biosphere–atmosphere interactions over West Africa. II: Multiple climate equilibria, Q. J. Roy. Meteorol. Soc., 126, 1261–1280, 2000. 1552
Willis, K. and McElwain, J.: The Elvolution of Plants, Oxford University Press, m300116, 2002. 1553, 1554

CPD
11, 1551–1578, 2015

Wolfe, J.: Distribution of major vegetation types during the Tertiary, in: The Carbon Cycle and Atmospheric CO_2: Natural Variations Archean to Present, edited by: Sundquist, E. T., and Broecker, W. S., American Geophysical Union, Washington/DC, 357–375, 1985. 1553, 1554

Zachos, J., Berza, J., and Wise, S.: Early Oligocene ice-sheet expansion on Antarctica – stable isotope and sedimentological evidence from Kerguelen Plateau southern Indian-Ocean, Geology, 20, 569–573, 1992. 1553

Zachos, J., Pagani, M., Sloan, L., Thomas, E., and Billups, K.: Trends, rhythms, and aberrations in global climate 65 Ma to present, Science, 292, 686–693, 2001. 1555

Zeng, N. and Neelin, D. J.: The role of vegetation–climate interaction and interannual variability in shaping the African Savanna, J. Climate, 13, 2665–2670, 2000. 1552

CPD
11, 1551–1578, 2015

Table 1. List of Plant Functional Types (PFTs) defined in the land surface scheme JSBACH.

Plant Functional Type
Tropical evergreen trees
Tropical deciduous trees
Extra-tropical evergreen trees
Extra-tropical deciduous trees
Raingreen shrubs
Cold shrubs
C_3 grass
C_4 grass

CPD
11, 1551–1578, 2015

Table 2. Boundary conditions in the early Eocene climate simulations and in the pre-industrial climate simulations.

	Pre-industrial	Early Eocene
CO_2 concentration	280 ppm	560 ppm
Methane	0.8 ppm	0.8 ppm
Nitrous oxide	0.288 ppm	0.288 ppm
Orbit	pre-industrial	pre-industrial
Bathymetry and orography	present-day	Bice and Marotzke (2001)
Ice sheets	pre-industrial	none

CPD
11, 1551–1578, 2015

Table 3. Simulations included in the experiment. The same set of simulations is performed for the early Eocene climate and for the pre-industrial climate. For both climates, the simulations differ concerning the initial vegetation–atmosphere state. The simulations start either from the forest world or from the dark desert world simulated by Port et al. (2015). Soils have a homogeneous soil albedo of 0.1.

	Initial state	Boundary conditions
FP	**F**orest world	**P**re-industrial
DP	**D**esert world	**P**re-industrial
FE	**F**orest world	**E**arly Eocene
DE	**D**esert world	**E**arly Eocene

CPD
11, 1551–1578, 2015

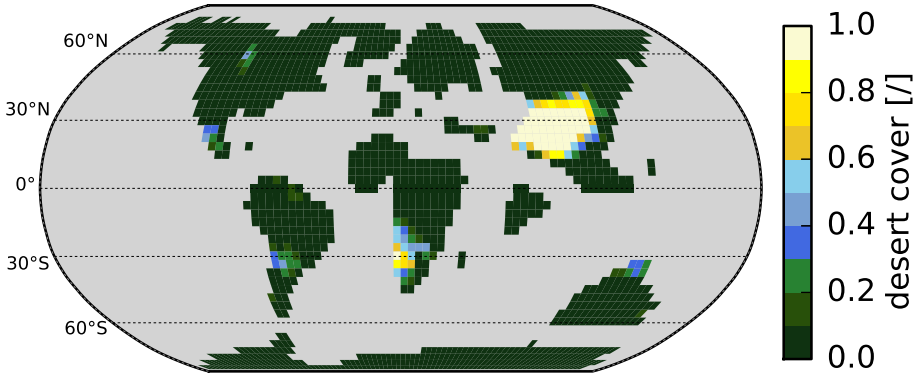

Figure 1. Desert cover in the DE simulation. The average over the last 30 years of the simulation is shown. Green indicates a minimum desert cover. Blue refers to semi-desert conditions. Yellow marks desert regions.

CPD
11, 1551–1578, 2015

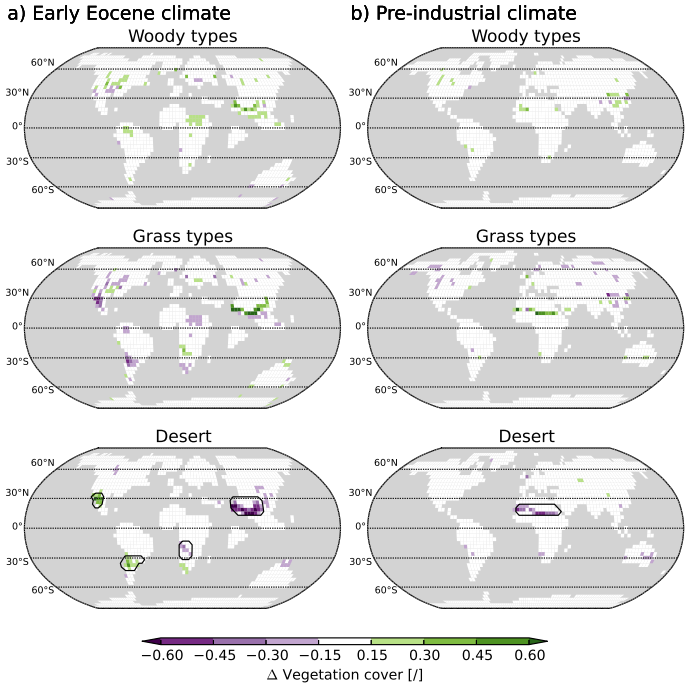

Figure 2. Differences in vegetation cover between the simulations that start from a forest world and the simulations that start from a desert world. Shown are differences for the early Eocene climate (FE – DE) **(a)** and for the pre-industrial climate (FP – DP) **(b)**. Mapped differences refer to the average over 30 years and are significant on a 95 % level. Woody types include all trees and shrubs. Grass types refer to C_4 grass and to C_3 grass. Green colours indicate a higher cover fraction in the FD than in the DD simulation. Purple colours refer to a smaller cover fraction in the FD simulation. Black contour lines mark regions which are analysed in more detail in Figs. 3 and 7.

CPD
11, 1551–1578, 2015

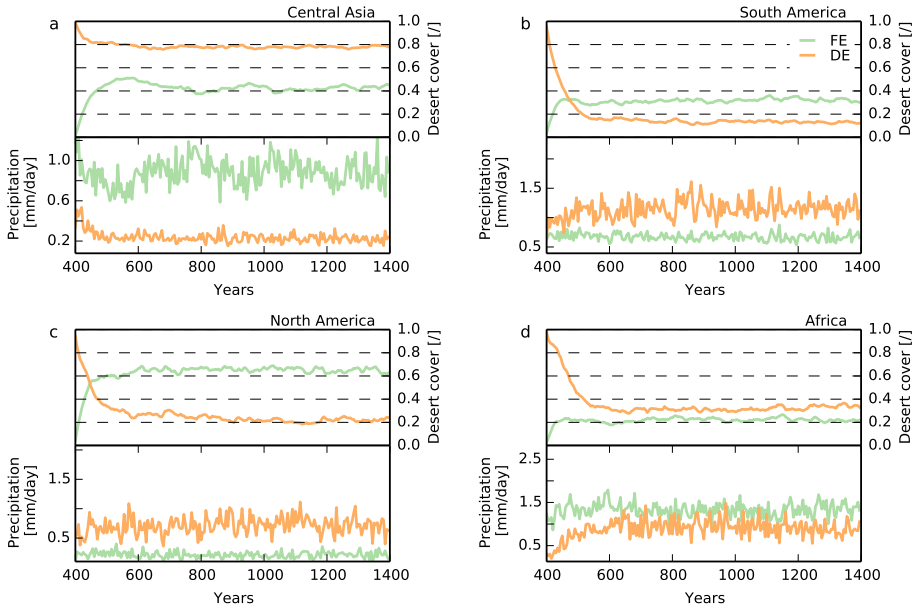

Figure 3. Time series of desert cover and precipitation in selected regions in Central Asia **(a)**, South America **(b)**, North America **(c)**, and Africa **(d)** in the FE simulation (green line) and in the DE simulation (orange line). The regions are marked in Fig. 2. Both time series show five-year mean values.

CPD
11, 1551–1578, 2015

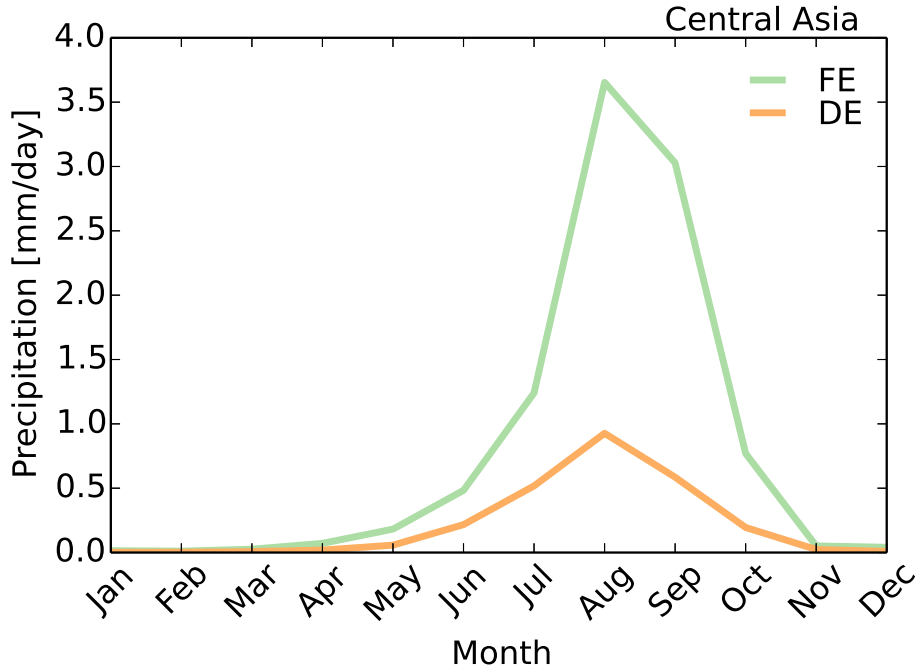

Figure 4. Annual cycle of precipitation in early Eocene Central Asia. The respective region is marked in Fig. 2. Lines refer to the FE simulation (green) and the DE simulation (orange). The average over the last 30 years of each simulation is considered.

CPD
11, 1551–1578, 2015

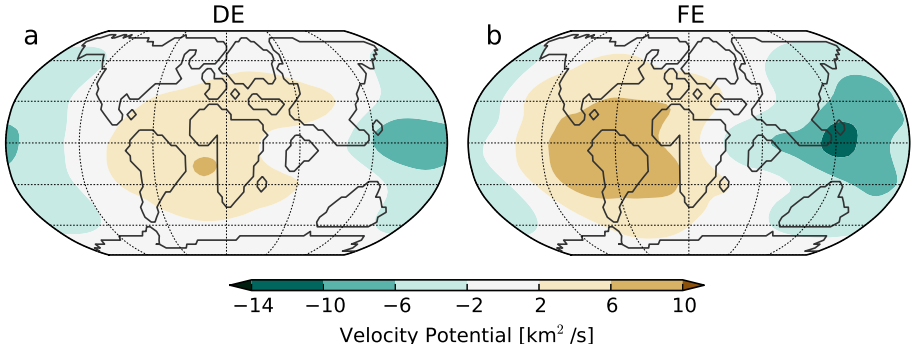

Figure 5. Velocity potential at 200 hPa in the DE simulation **(a)** and in the FE simulation **(b)**. The average over the last 30 years of the simulations is shown. Brown colours indicate to a positive velocity potential, upper-air convergence, and subsidence. Green colours indicate to a negative velocity potential, upper-air divergence, and rising.

CPD
11, 1551–1578, 2015

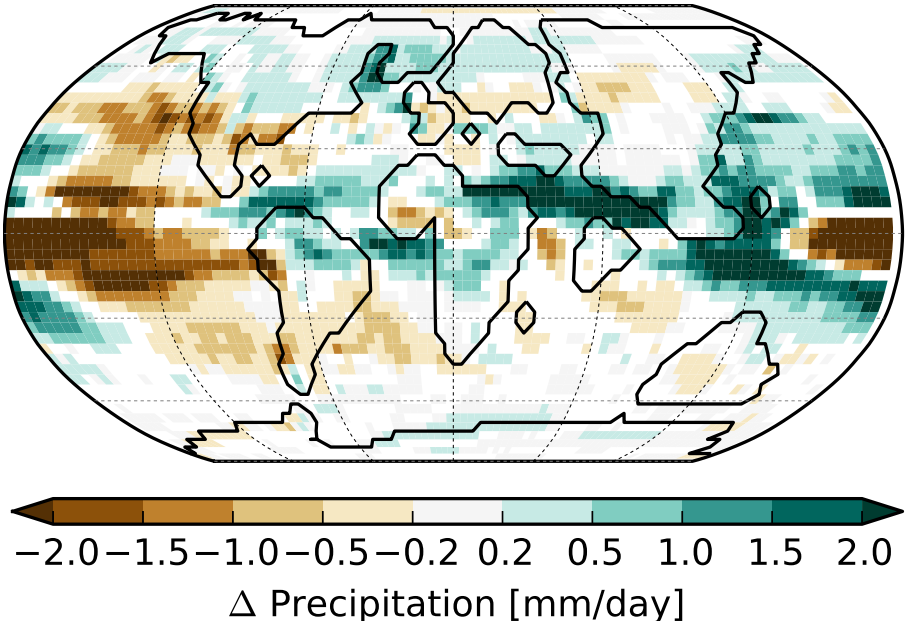

Figure 6. Precipitation differences between the FE simulation and the DE simulation. The average over the last 30 years of the respective simulation is considered. Depicted differences are significant on a 95 % level.

CPD
11, 1551–1578, 2015

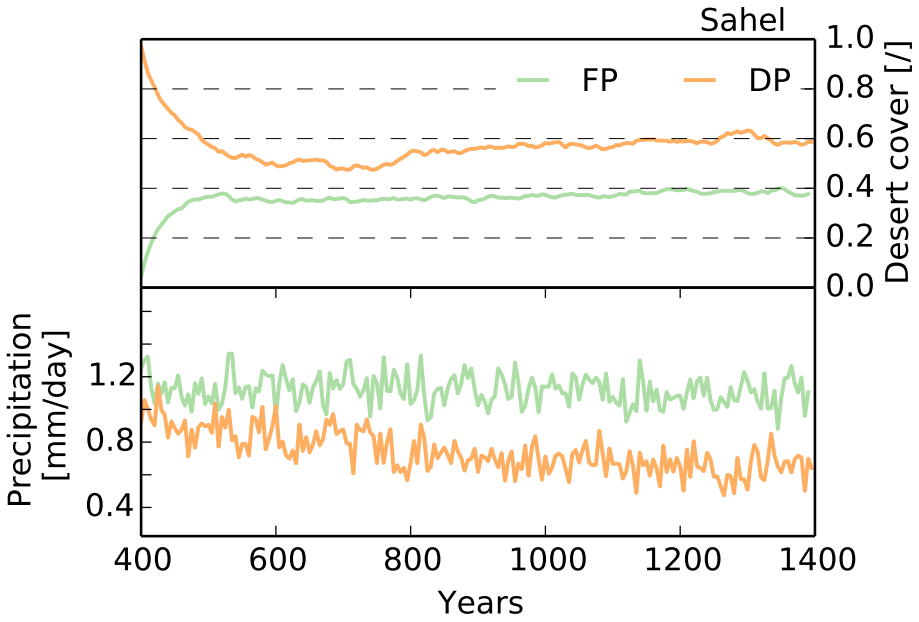

Figure 7. Time series of desert cover and precipitation in pre-industrial Sahel in the FP simulation (green line) and in the DP simulation (orange line). The Sahel region is marked in Fig. 2. Both time series show five-year mean values.

CPD
11, 1551–1578, 2015

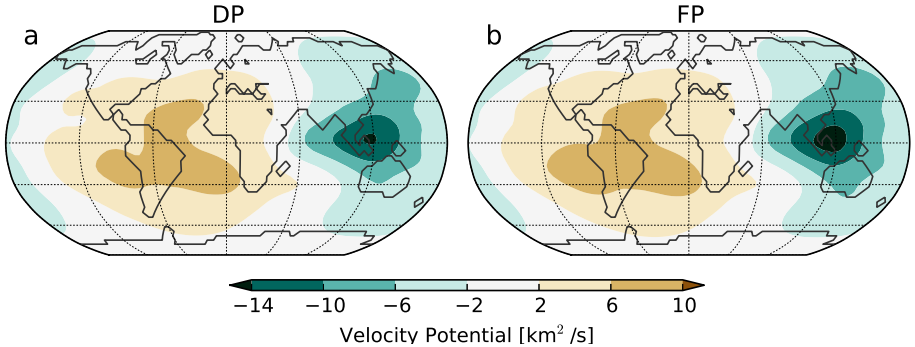

Figure 8. Velocity potential at 200 hPa in the DP simulation **(a)** and in the FP simulation **(b)**. The average over the last 30 years of the simulations is shown. Brown colours indicate to a positive velocity potential, upper-air convergence, and subsidence. Green colours indicate to a negative velocity potential, upper-air divergence, and rising.

CPD
11, 1551–1578, 2015

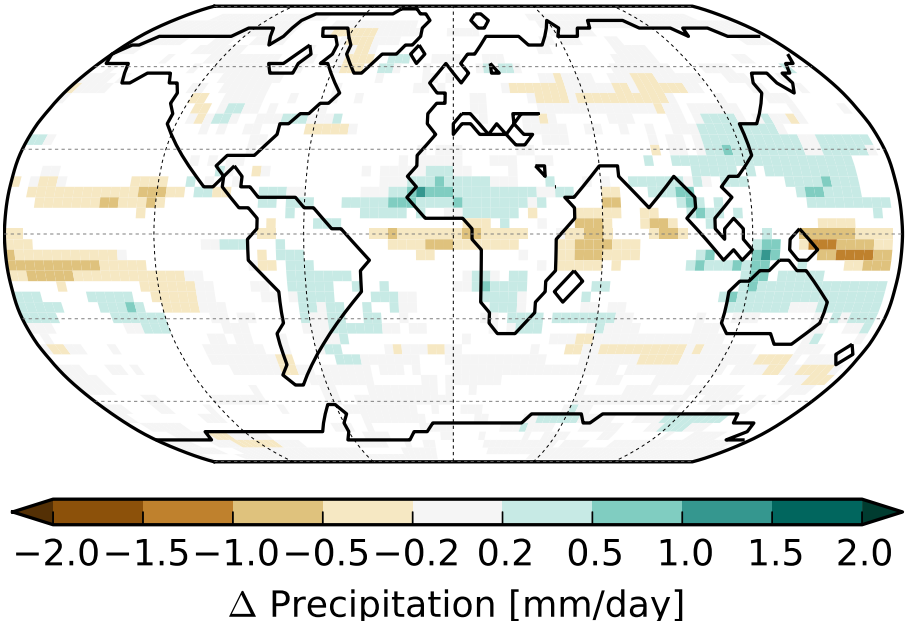

Figure 9. Precipitation differences between the end of the FD_P simulation and the end of the DD_P simulation. Depicted differences are significant on a 95 % level.

CPD
11, 1551–1578, 2015